AIMS Biophysics, 3 (4): 479-500.
DOI: 10.3934/biophy.2016.4.479
Received: 30 August 2016
Accepted: 13 October 2016
Published: 24 October 2016

http://www.aimspress.com/journal/biophysics

Research article

Interplay of vacuolar transporters for coupling primary and secondary active transport

Michèle Siek, Berenice Marg, Chris M. Ehring, Derya Kirasi, Michael Liebthal and Thorsten Seidel *

Dynamic Cell Imaging, Faculty of Biology, Bielefeld University, 33501 Bielefeld, Germany

*** Correspondence:** Email: thorsten.seidel@uni-bielefeld.de; Tel: +49 521-106-5588.

Abstract: Secondary active transporters are driven by the proton motif force which is generated by primary active transporters such as the vacuolar proton pumps V-ATPase and V-PPase. The vacuole occupies up to 90 % of the mature cell and acidification of the vacuolar lumen is a challenging and energy-consuming task for the plant cell. Therefore, a direct coupling of primary and secondary active transporters is expected to enhance transport efficiency and to reduce energy consumption by transport processes across the tonoplast. This has been addressed by analyzing physical and functional interactions between the V-ATPase and a selection of vacuolar transporters including the primary active proton pump AVP1, the calcium ion/proton exchanger CAX1, the potassium ion/proton symporter KUP5, the sodium ion/proton exchanger NHX1, and the anion/proton exchanger CLC-c. Physical interaction was demonstrated *in vivo* for the V-ATPase and the secondary active transporters CAX1 and CLC-c, which are responsible for calcium- and anion-accumulation in the vacuole, respectively. Measurements of V-ATPase activity and vacuolar pH revealed a functional interaction of V-ATPase and CAX1, CLC-c that is likely caused by the observed physical interaction. The complex of the V-ATPase further interacts with the nitrate reductase 2, and as a result, nitrate assimilation is directly linked to the energization of vacuolar nitrate accumulation by secondary active anion/proton exchangers.

Keywords: vacuolar ATPase; proton motif force; secondary active transport; vacuole; protein-protein interaction

1. Introduction

With up to 90% of the cellular volume the plant vacuolar system represents the largest compartment group within plant cells and serves as storage compartment, disposal for waste and toxins, lytic compartment, Ca^{2+}-store, and represents an important factor for plant growth and apoptosis [1,2]. These multiple functions require a versatile transport system at the tonoplast. In particular, ion influx and efflux have to be coordinated to ensure proper functionality of the cell. For instance, the cytosolic concentration of calcium ions requires a tight regulation to allow for signal-induced calcium ion release and to maintain a low level of calcium ions in resting non-stimulated cells [3]. Primary active and outward directed Ca^{2+}-pumps are crucial for the resting state, secondary active transporter for the termination of Ca^{2+}-signaling [4]. Another example is the transient nitrate storage to prevent excessive production of cytotoxic nitrite as a result of the nitrate assimilation. Due to the nitrate accumulation in the vacuole, the transport is directed against the concentration gradient so that active transport is required to enable the nitrate deposition in the vacuole [5]. Secondary active transporters such as the calcium ion/proton exchanger CAX1 and anion/proton exchangers of the CLC-family mediate calcium and nitrate transport out of the cytosol into the vacuole [4,6]. Therefore, the formation of a proton motif force (pmf) is essential to energize the secondary active transporters. This pmf is created by the vacuolar-type proton translocating ATPase (V-ATPase) and the vacuolar proton-translocating pyrophospatase (V-PPase) [7]. While the dimeric V-PPase uses a byproduct of the cellular metabolism as energy source, the multimeric enzyme complex V-ATPase consumes comparatively valuable ATP [8]. As a consequence, the V-ATPase activity is linked to ATP- and glucose availability [9]. Besides the co-existence of V-PPase and V-ATPase in mature vacuoles, it is widely accepted that their relationship is altered during plant development. The V-PPase pumps protons into vacuoles during embryo and seedling development, the V-ATPase takes over with increasing age of the plant cell and becomes the dominant proton pump for vegetative growth [10,11]. This arrangement pays attention to the availability of ATP and PP_i during development and might be also a consequence of the complex structure of the V-ATPase: The V-ATPase is a multimeric complex of more than 800 kDa, which can be divided into a membrane integral sector V_O (subunits VHA-a, VHA-c, VHA-c", VHA-d, VHA-e) and a membrane associated sector V_1 (subunits VHA-A–VHA-H) [2]. The V_O-sector is dominated by a rotating ring of approximately six copies of the proteolipids VHA-c/VHA-c". The C-terminal half of VHA-a resides next to the proteolipid ring and provides half channels so that cytosolic protons have access to their binding sites at VHA-c and can be released into the vacuolar lumen [12]. The rotation of the proteolipids is driven by sequential ATP-hydrolysis within the three copies of VHA-A, which form the hexameric head together with three copies of VHA-B. VHA-D and VHA-F form the central stalk and transduce the sequential conformational alterations of VHA-A into rotation [12]. The peripheral subunits VHA-C, VHA-E, VHA-G and VHA-H form a complex stator structure which prevents co-rotation of the head and anchors the V_1-sector to the membrane via the N-terminal domain of VHA-a [2]. Recent work revealed a growing number of additional proteins interacting with the V-ATPase and likely regulating its activity. For instance, a glycolytic aldolase interacts with the V-ATPase in a gibberellin-dependent manner in rice [13,14], following blue light perception a regulatory 14-3-3 protein binds to the phosphorylated VHA-A subunits and activates the V-ATPase, and thus, links the V-ATPase activity to day light [15]. Kinases such as the WNK8 in *Arabidopsis thaliana* and CDPK1 in barley phosphorylate individual VHA-subunits such as VHA-a, VHA-C, and

VHA-A [15–18]. Additional evidence for an extensive V-ATPase protein interaction network derives from yeast, where the V-ATPase interacts with the cytoskeleton, the RAVE-complex, proteins of the VTC-family, and shows cooperated activity with the cation transporter Vnx1p and Ca^{2+}-releasing channels [19–25]. Functional coupling of the secondary active transporter CAX1, NHX1 and the V-ATPase has been observed in plants, too, but a physical interaction was only proven for the canonical vacuolar proton pumps V-PPase and V-ATPase in *Kalanchoë blossfeldiana* [7].

The V-ATPase subunits VHA-c"1 (23), VHA-d1 (2), VHA-d2 (1), VHA-e1 (54), VHA-B3 (1), VHA-C (7), VHA-E1 (3), VHA-G2 (1), VHA-G3 (3), VHA-H (1) were further included in a large scale screening for interaction partners and regulators of membrane integral proteins using the mating-based split-Ubiquitin system (mbSUS), a yeast-2-hybrid system that has been optimized for the analysis of membrane proteins. The numbers in brackets provide the number of identified interaction partners [26]. A previous attempt by the Arabidopsis Interactome Mapping Consortium applied the conventional yeast-2-hybrid system and included the V-ATPase subunits VHA-A (3), VHA-B1 (4), VHA-B2 (1), VHA-B3 (1), VHA-C (5), VHA-D (2), VHA-E1 (1), and VHA-G1 (1), the obtained data on membrane integral proteins of the V_O-sector is omitted here due to the nature of the yeast-2-hybrid system [27]: The common yeast-2-hybrid system relies on the nuclear import of the interaction partners to initiate the expression of reporter genes. The published data suggests that the identity of many proteins involved in the active state of the V-ATPase and its regulation is still elusive. However, the large-scale analyses were performed in yeast and obtained interactions might not be valid in plants, either due to a differential expression or due to the distinct cellular environment in yeast. Therefore, we aimed at the investigation of functional and physical interactions in this work and focused mainly on data obtained in plants.

2. **Materials and Methods**

2.1. Plant material and growth conditions

A. thaliana (Columbia) was grown on soil in a growth chamber with 12 h light (240 µmol quanta m^{-2} s^{-1}, 19 °C) and 12 h dark (18 °C) with 60% relative humidity. The hypocotyl-derived cell suspension culture At7 [28] was applied for localization studies and physiological analysis. The cells were cultivated at 26 °C upon shaking in the dark. 3 g of cells were transferred weekly to 45 ml MS-media: 0.43% (w/v) Murashige and Skoog basal salt mixture (Sigma-Aldrich M5524), 0.1% Gamborg B5 Vitamin stock (Sigma-Aldrich), 3% sucrose, 0.1 ‰ 2,4-dichlorophenoxyacetatic acid, adjusted to pH 5.7. The MS-media contained 18.8 mM KNO_3 and 20.61 mM under control conditions. For nitrate-dependent experiments the media was prepared with the indicated concentrations of KNO_3 and without NH_4NO_3 as nitrogen source.

The transgenic insertion lines SALK_105121C (NHX1), SALK_120707C (KUP5), SALK_115644C (CLC-c), SALK_106153C (AVP1) SALK_021486C (Cax1) were generated by the Salk Institute for Biological Studies, department of plant biology, [29] and obtained from the Nottingham Arabidopsis Stock Center (NASC).

2.2. Crosslinking and co-immunoprecipitation

Formaldehyde-crosslinking was performed in At7 protoplasts. Cells were incubated for 20 min in 1% formaldehyde with repeated inverting at room temperature in the dark. Approximately 300 µl of cell suspension were mixed with 300 µl of 2% formaldehyde in PBS. Next, the cells were centrifuged for 10 min at 4 °C and 10,000 × g. The Pierce® co-immunoprecipitation kit (Thermo Scientific, Kit-No. 26149) was applied for co-immunoprecipitation according to the manufacturer's protocol: Briefly, an antibody directed against VHA-A and VHA-E was immobilized by a 2.5 h incubation with the resin to ensure proper coupling. The pelleted cells were washed in PBS, resuspended in lyse/wash-buffer and incubated for 5 min under mixing at RT. The sample was centrifuged again, the supernatant transferred to a column with the immobilized antibody/resin mix and incubated overnight while mixing at 4 °C. The proteins were finally eluted and subjected to SDS-PAGE in preparation for mass spectroscopy.

2.3. Mass spectroscopy

Protein bands were excised from SDS-gels and transferred to emollient-free reaction tubes and were washed twice with 200 µl 30% acetonitrile in 0.1 M ammonium hydrogen carbonate for 10 min. The gel-slices were dried in a vacuum-concentrator for 30 min. The tryptic digestion was done with 0.1 µg/µl trypsin in 10 mM ammonium bicarbonate for 30 to 45 min at RT. 20 µl 10 mM ammonium bicarbonate were added to each gel slice to prevent drying and the samples were incubated overnight at 37 °C. After complete evaporation, the samples were rehydrated in 15 µl 50% acetonitrile, 0.1% TFA. 1 µl of the peptide sample was finally plotted on the MTP Anchorchip™ 384 TF (Bruker). Briefly, before the peptide sample was dried, 1 µl of the HCCA matrix was added (0.2 mg · ml^{-1} α-Cyano-4-hydroxycinnamic acid in 90% acetonitrile, 0.1% TFA and 0.1 M $NH_4H_2PO_4$). After complete evaporation the mass spectra of the peptide samples were obtained with a MALDI-TOF MS/MS (Ultraflextreme, Bruker) in MS-mode and analysed by the Mascot software (Matrix science, UK). The settings were trypsin as the enzyme, no more than one missed cleavage and a peptide tolerance of 100 ppm. The Mascot-score is defined as -10×Log(P) with P as probability of a false positive match to a database. The threshold further depends on the background noise. For the settings used in this analysis, the probability of a false positive match is smaller than 0.05 for proteins showing a Mascot-score of more than 58.

2.4. Isolation of tonoplasts and V-ATPase activity measurements

Tonoplasts were isolated as described before [30]. The tonoplast suspension was supplemented with Brij58 (50 mM Tricine, pH 8.0, 20% (v/v) Glycerol, 2% (w/v) Brij58) resulting in a V-ATPase/detergent ratio of 1:10 and incubated for 30 min at 4 °C. The samples were centrifuged at 98,000 × g and 4 °C. The supernatant contained the solubilised V-ATPase. The activity was measured by recording the released phosphate according to Bencini with modifications as described by Dietz et al. (1998) [30,31]. Bafilomycin-sensitive ATP hydrolysis corresponds to V-ATPase activity, to this end 2.8 µM Bafilomycin was added to the reaction and related to a parallel reaction without Bafilomycin.

2.5. Molecular biology

For genotyping, one leaf was ground with a micro-pistil in a 1.5 ml reaction tube for 10 s, 500 µl Edwards-buffer (200 mM Tris-HCl pH 7.5, 250 mM NaCl, 25 mM EDTA, 0.5% SDS) was given to the samples and grinding was continued. Subsequent vortexing, the samples were centrifuged for 2 min at 10,000 × g and 300 µl of the supernatant were given to 310 µl isopropanol to precipitate the DNA. Precipitation was performed by incubation at RT for 10 minutes and centrifugation at 10,000 × g for 7 min. The pellets were resuspended in 100 µl sterile water. The actual genotyping was performed by polymerase chain reaction (PCR) using the DNA-polymerase from *Thermus aquaticus* (Taq-Polymerase). A set of three oligo nucleotides was applied for each reaction. The oligo "LBb1" binds to the DNA-insertion, the "LP"- and "RP"-oligo bind the genomic DNA flanking the insertion (for oligo-information see table 1). Homozygous insertion lines are characterized by a PCR-product of either LBb1 and LP or LBb1 and RP, depending on the orientation of the insertion. The wildtype shows a PCR-product of LP and RP, heterozygous lines show both types of PCR-products. Oligo sequences were obtained with the primer design tool from the Salk Institute Genomic Analysis Laboratory (SIGnAL) which suggests sequences for genotyping of SALK-lines (signal.salk.edu/tdnaprimers.2.html).

Table 1. Oligo nucleotides for genotyping.

Oligo	Sequence (5'–3')	Insertion line	Transporter
LBb1	GCGTGGACCGCTTGCTGCAACT	n.a.	n.a.
NHX1_LP	TTGAGGTAACAACGCTTGGTC	SALK_105121C	NHX1
NHX1_RP	GGTGGATCTGATCTGAATTGC	SALK_105121C	NHX1
Hak5_LP	TCCCAAATCAACTTCCATCAG	SALK_120707C	KUP5
Hak5_RP	CAGCAAGAGGCAAGGTAACAC	SALK_120707C	KUP5
CAX1_LP	CTAGTTGCCTGCACGAGAATC	SALK_021486C	Cax1
CAX1_RP	AACCGCTCACAACATGTCTTC	SALK_021486C	Cax1
AVP1_LP	CATCATCAAACAACCACCAATC	SALK_106153C	AVP1
AVP1_RP	TGGCCTGTTTTAATTAAAGGG	SALK_106153C	AVP1
CLCc_LP	AAGTTGCCGGAAAAGAATAGC	SALK_115644C	CLC-c
CLCc_RP	ACCTTGTGGACAAAGTCCTCC	SALK_115644C	CLC-c

The plasmids 35S-EYFP-C and 35S-ECFP-C [32] were applied for localization studies and Förster resonance energy transfer (FRET)-analyses [32,33,34]. Briefly, FRET describes a dipole-dipole coupling which results in radiation-less energy transfer between the so-called donor molecule and the acceptor molecule. Prerequisites are a proper orientation of the dipoles, a distance of typically less than 10 nm as well as a high spectral overlap of the donor's emission spectrum and the acceptor's absorption spectrum. A donor-acceptor pair is called a "FRET-pair" and is characterized by its Förster radius R_0. R_0 is the distance of half maximal energy transfer between both molecules [34]. Here, cyan fluorescent proteins served as donor and yellow fluorescent proteins as acceptors. The coding sequences (cds) of the analyzed proteins were obtained from The Arabidopsis Information Resource (TAIR, https://arabidopsis.org) using the Arabidopsis locus identifiers according to the Arabidopsis genome initiative (AGI): AT2G38170 (Cation Exchanger 1, CAX1), AT1G15690 (Arabidopsis Vacuolar Pyrophosphatase 1, AVP1), AT5G49890 (Chloride Channel C, CLC-c), AT4G33530 (K^+ Uptake Permease 5, KUP5), AT5G27150 (Na^+/H^+ Exchanger 1, NHX1)

and AT1G37130 (Nitrate Reductase 2, NR2). The coding sequences were amplified by PCR using oligo nucleotides with flanking NotI/EcoRI (CAX1, AVP1, NR2) or NotI/StuI (CLC-c, KUP5, NHX1) restriction sites (for oligo-information see table 2). Subsequent a reaction with restriction enzymes, the fragments were used for ligation with the plasmid 35S-EYFP-C. Within 35S-VHA-c3-EYFP [31], the EYFP has been replaced by mTurquoise2 for FRET-analyses of the protein pairs CAX1/VHA-c3 and VHA-c3/VHA-c3.

For mbSUS analysis, the cloning was started with Gateway® entry clones made from attB-flanked PCR-products without stop codon (for oligo-information see table 2) and the plasmid pDONR221 following the manufacturer's instructions (Invitrogen). The LR clonase (Invitrogen) was employed to transfer the VHA-A and VHA-E coding sequences to the pX-NubWTgate-vector and the coding sequences of CLC-c and NR2 to the pMetYCgate-vector.

2.6. Mating-based split Ubiquitin system

The yeast strains THY.AP4 (*MATa ura3, leu2, lexA::LacZ::trp1 lexA::HIS3 lexA::ADE2*) and THY.AP5 (*MATα URA3*, *leu2*, *trp1*, *his3 loxP*::*ade2*) were transformed with the pX-NubWTgate and pMetYCgate vectors [35], respectively, using the LiAc-protocol (modified of Gietz et al., 1995 [36]). THY.AP4 and THY.AP5 were incubated on –Trp-plates and –Leu-plates, respectively. For mating, one colony of the Nub-construct and one of the Cub-construct were combined and grown overnight in 5 ml YPD. 15 µl of these cultures were selected for diploid cells on diploid media and then screened for robust interactions on interaction media. In both cases the plates were incubated for two days at 30 °C. Finally, overlay assays were performed with X-gal to confirm the interactions [35]. The composition of the yeast media was described by Obrdlik et al. (2004) and Ludewig et al., (2003) [35,37].

2.7. Protoplast transfection

Leaves were harvested from soil grown *Arabidopsis thaliana* plants at the age of about four weeks. Protoplasts were isolated as described before [38]. Protoplast isolation of At7-cells was performed according to Appelhagen et al. (2010) [39]. Transfections were performed in uncoated hydrophobic 8-well slides (Ibidi, Martinsried Germany): 20 µl of protoplast suspension were mixed with 5 µl of plasmid DNA and 25 µl of PEG-solution (40% PEG4000, 2.5 mM $CaCl_2$, 0.2 M mannitol) and incubated for 10 min in the dark. The assay was diluted stepwise with 50 µl, 100 µl and two times 200 µl of W5-solution (154 mM NaCl, 2.5 mM $CaCl_2$, 5 mM glucose, 5 mM MES pH 5.7). In between, the cells were incubated for 10 min. The transfected cells were kept in the dark at 25 °C prior to microscopic analysis.

2.8. Quantitative microscopy

The vacuolar pH was measured with a Leica SP2 confocal laser scanning microscope. Cells were loaded with 5 µM 6-carboxy fluorescein diacetate and the fluorescence was detected with photomultiplier 2 in the range of 500 to 530 nm. The dichroic mirror RSP500 and a water-dipping objective with 40-fold magnification were used. The probe was excited sequentially with the 458 nm

and 488 nm line of an argon ion laser, the laser power was adjusted to equal emission intensity at pH 7. Calibration and data evaluation were performed as described before [9,33].

Table 2. Oligo nucleotides for cloning.

Oligo	Sequence (5' – 3')	AGI (name) direction, enzyme
CAX1_NotF	AAAA GCGGCCGC ATG GCG GGA ATC GTG ACA	At2g38170 (Cax1) forward, NotI
CAX1-Eco_r	TTTTT GAATTC TTA ACC CGT TTT AAC TTT	At2g38170 (Cax1) reverse, EcoRI
PM-ATPase_NotF	AAAA GCGGCCGC ATG TCA GGT CTC GAA GAT	At2g18960 (AHA1) forward, NotI
PM-ATPase_EcoR	TTTTT GAATTC TAC ACA GTG TAG TGA TG	At2g18960 (AHA1) reverse, EcoRI
Ppase_NotF	AAAA GCGGCCGC ATG GTG GCG CCT GCT TTG	At1g15690 (AVP1) forward, NotI
Ppase_EcoR	TTTTT GAATTC TAG AAG TAC TTG AAA AG	At1g15690 (AVP1) reverse, EcoRI
CLC_c_F-Not1	AAAA GCGGCCGC ATG GAT GAT CGG CAC GAA GGA G	AT5G49890 (CLC-c) forward, NotI
CLC_c_rev-Stu1	TTTTT AGGCCT TCA CTT GAG GGG ATC AAT GTG AGG G	AT5G49890 (CLC-c) reverse, StuI
Hak5-for-Not1	AAAA GCGGCCGC ATG TTT CAC GTG GAA GAA GAA AGC	AT4G33530 (HAK5 / KUP5) forward, NotI
Hak5-rev-Stu1	TTTT AGGCCT TCA TAC CAT ATA AGT CAT TCC	AT4G33530 (HAK5 / KUP5) reverse, StuI
NHX1-for-Not1	AAAA GCGGCCGC ATG TTG GAT TCT CTA GTG TCG	AT5G27150 (NHX1) forward, NotI
NHX1-rev-Stu1	TTTT AGGCCT TCA AGC CTT ACT AAG ATC AGG AGG G	AT5G27150 (NHX1) reverse, StuI
A-Yeast-for	GGGGACAAGTTTGTACAAAAAAGCAGGCTTC ATG CCGGCGTTTTACGGAGG	At1g78900 (VHA-A)
A-Yeast-rev	GGGGACCACTTTGTACAAGAAAGCTGGGTG TTC CCGAGTTTCATCTTC	At1g78900 (VHA-A)
E1-Yeast-for	GGGGACAAGTTTGTACAAAAAAGCAGGCTTC ATG AACGACG GAGATGT	At4g11150 (VHA-E1)
E1-Yeast-rev	GGGGACCACTTTGTACAAGAAAGCTGGGTG TCC GGCAGTAACTTGGC	At4g11150 (VHA-E1)
NR-Yeast-for	GGGGACAAGTTTGTACAAAAAAGCAGGCTTC ATG GCGGCCTCTGTAGAT	AT1G37130 (NR2)
NR-Yeast-rev	GGGGACCACTTTGTACAAGAAAGCTGGGTG CTC GAATATCAAGAAATCC	AT1G37130 (NR2)
CLC-Yeast-for	GGGGACAAGTTTGTACAAAAAAGCAGGCTTC ATG GATGATCGGCACGAAG	AT5G49890 (CLC-c)
CLC-Yeast-rev	GGGGACCACTTTGTACAAGAAAGCTGGGTG TCC CTTGAGGGGATCAATG	AT5G49890 (CLC-c)

Confocal localization analyses were performed using a Leica SP2 or Zeiss LSM780 microscope as described before [32,34]. ECFP (mTurquoise2), EYFP and the chlorophyll autofluorescence were detected in the range of 470–510 nm, 530–600 nm, 650–700 nm, respectively. Cyan fluorescent proteins (ECFP, mTurquoise2) and EYFP were excited using the 458 nm laser line and the 514 nm lines of an argon ion laser, respectively. Chlorophyll was excited with the 458 nm line, too, and

transmitted light images were obtained with the 458 nm line. Main beam splitters were applied that allow for sequential excitation with the 458 nm and 514 nm laser line so that tracks were alternating line by line. Images were recorded with one- to four-fold line-averaging and the intensity resolution was 12 bits / pixel. The settings were identical for FRET-measurements, but the signal amplification was strictly defined and kept constant.

2.9. Statistical analysis

Arithmetic mean and standard deviation were calculated for all datasets. For some datasets the standard error was calculated, too, and given in the figures (see legends). Variances of the data were compared by F-test. The non-parametric Mann-Whitney-U-test was applied for the data on vacuolar pH and the effects of KNO_3 and bafilomycin on plant cell suspension culture. The student's t-test was applied for the statistical analysis of the V-ATPase activity. A significant difference was accepted for $p \leq 0.05$.

2.10. In silico-analysis

Predictions of transmembrane domains were obtained from Aramemnon [40]. Co-Expression data were collected from the ATTED II-database (http://atted.jp). The ATTED II-database comprises data from Affymetrix microarray-analysis and thus, contains information on transcript abundance [41]. To quantify the degree of co-expression for genes that are co-expressed with the query gene, the correlation coefficients R are calculated and the genes are listed with decreasing R so that the co-expressed genes get rank numbers. The same procedure was performed with the thereby identified co-expressed genes as query to obtain the rank number of the initial query gene. The MR-value of a gene pair is given as the square root of the product of both rank numbers. Data on subcellular localization and organ specificity was obtained from MASCP Gator (http://gator.masc-proteomics.org/). This database contains data from GFP-localization experiments and mass spectroscopy of samples from *A. thaliana*. These samples were either tissue- or organelle-specific. [42]. Predictions of subcellular localization were collected from the BAR Arabidopsis eFP-browser [43].

3. **Results**

3.1. Selection of initial candidates

The secondary active transporters CAX1 (AT2G38170) and NHX1 (AT5G27150) as well as the proton pump AVP1 (AT1G15690) were reported to interfere with the V-ATPase activity and therefore suggested to interact with the V-ATPase [6,44,45,46]. An ATTED II co-expression analysis [41] for the vacuolar V-ATPase subunit VHA-a3 identified the secondary active transporters KUP5 (AT4G33530), a potassium transporter, and CLC-c (AT5G49890), an anion/proton antiporter (Figure 1). These transporters showed low MR-values for a high number of V-ATPase subunits. MR-values were classified based on the MR-values between the genes encoding for V-ATPase subunits. Finally, the available published data on CAX1, NHX1, AVP1 and the co-expression analysis resulted in the selection of the transporters CAX1, NHX1, AVP1, KUP5 and CLC-c. Crosslinking followed

by immunoprecipitation with an antibody directed against VHA-A was performed to identify transporters that are in a proximity close enough for the formaldehyde linkage. The antibody directed against VHA-A was chosen, because VHA-A is part of the catalytic core complex and was successfully used before by the Lüttge group [7]. However, transporters were not identified, but nitrate reductase 2 (AT1G37130) was found with a Mascot-score of 59 that is higher than the background signal. The crosslinking product had an apparent molecular weight (mw) of approximately 170–180 kDa. Subtracting the molecular weight of NR2 (102.8 kDa) leaves 67.2–77.2 kDa what matches the mw of VHA-A which served as bait. Next, *in silico* analyses were performed to estimate the possibility of a physical interaction between nitrate reductase 2 and the V-ATPase. Aramemnon predicted a weak probability (0.12) for two transmembrane domains within NR2. Proteomic data obtained from the MASCP gator-database revealed localizations in cytosolic, vacuolar and plasma membrane fractions and revealed its presence in all tissues, so that an interaction between V-ATPase and NR2 is possible based on this data.

3.2. Protein-protein interactions of transporters

Before testing the possibility of a direct interaction between V-ATPase and other transporters the proteins were analyzed pairwise for co-localization in Arabidopsis mesophyll protoplasts. This analysis was performed to check if the analyzed proteins show an overlapping subcellular localization which allows for a physical interactions. Since the FRET-analysis was performed to investigate physical interactions between V-ATPase and other membrane-integral proteins, the co-localization and FRET-studies were performed with the membrane integral V_O-subunits VHA-a3 and VHA-c3. The V-ATPase subunit VHA-c3 co-localized with CAX1, NHX1, KUP5 while VHA-a3 co-localized with AVP1 and CLC-c (Figure 2). This data indicates the possibility of an interaction. To test the predicted interaction between the V-ATPase and the selected transporters, FRET-measurements were performed in Arabidopsis mesophyll protoplasts. FRET offers a higher distance range than formaldehyde-crosslinking or bimolecular fluorescence complementation and thereby allows monitoring close proximity of proteins and thus, proof of protein interaction without direct physical contact of the labeled termini.

The FRET-pairs ECFP/EYFP and mTurquoise2/EYFP were applied for the analysis. The pairs differ in their Förster-radii so that the distances were calculated to allow for the comparison of the data sets. It should be mentioned that these distances do not correspond to real distances since the fluorophores' orientation κ^2 is unknown. However, under the assumption that κ^2 is 0.66 on average, distances of less than 1.5-times R_0 were considered as proof of interaction according to Gadella and co-authors (1999) [47]. CAX1/VHA-c3 (5.64 ± 0.36), AVP1/VHA-a3 (6.78 ± 0.51), CLC-c/VHA-a3 (7.31 ± 0.495) showed distances below 1.5-times R_0 while KUP5/VHA-c3 (8.05 ± 1.97) and NHX1/VHA-c3 (7.90 ± 1.37) did not meet that criteria (Figure 3A). The combination VHA-c3/VHA-c3 and the direct fusion of ECFP-EYFP served as positive controls showing average distances of 6.06 ± 0.06 and 4.99 ± 0.35 nm, respectively (Figure 3A).

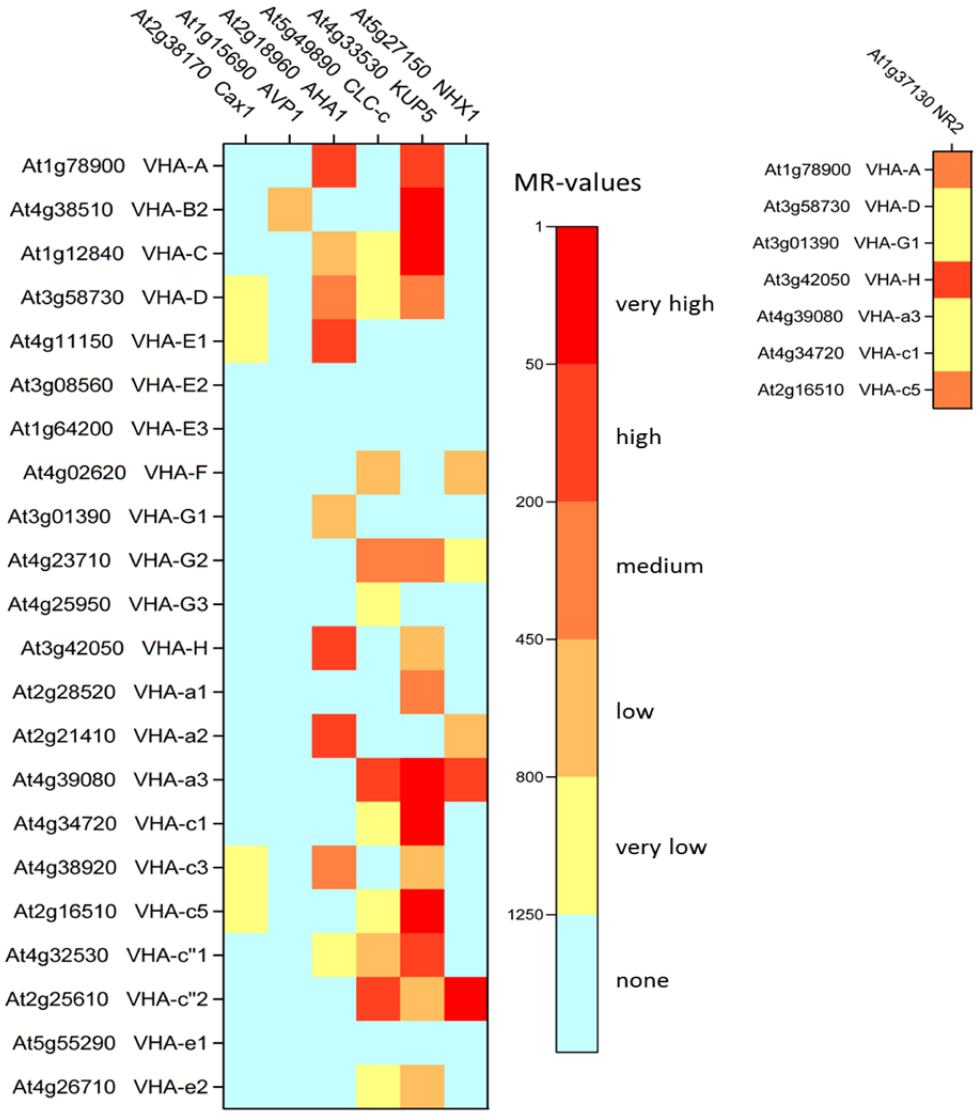

Figure 1. Co-expression of V-ATPase subunits and vacuolar transporters. Data was taken from ATTED II, the heat map bases on the MR-values as indicated in the legend bar. Co-expression of NR2 and V-ATPase subunits is given for a selection of subunits. The MR-value bases on the ranking of correlation coefficients R of the analyzed transcripts. Co-expressed genes are listed with decreasing R so that rank numbers can be assigned to the co-expressed genes. Then the co-expressed genes serve as query to obtain the rank number of the initial query gene. The MR-value is given as the square root of the product of both rank numbers.

In addition, the mating-based split-Ubiquitin system (mbSUS) was applied to investigate the interaction between the nitrate transporter CLC-c and the V-ATPase subunits VHA-A and VHA-E1 as well as the interaction between the nitrate reductase 2 and VHA-A/VHA-E1. The mbSUS depends on the bimolecular complementation of Ubiquitin in the cytosol. Once Ubiquitin is folded, Ubiquitin-dependent proteases cleave off a transcription factor which activates reporter genes [35]. The C-

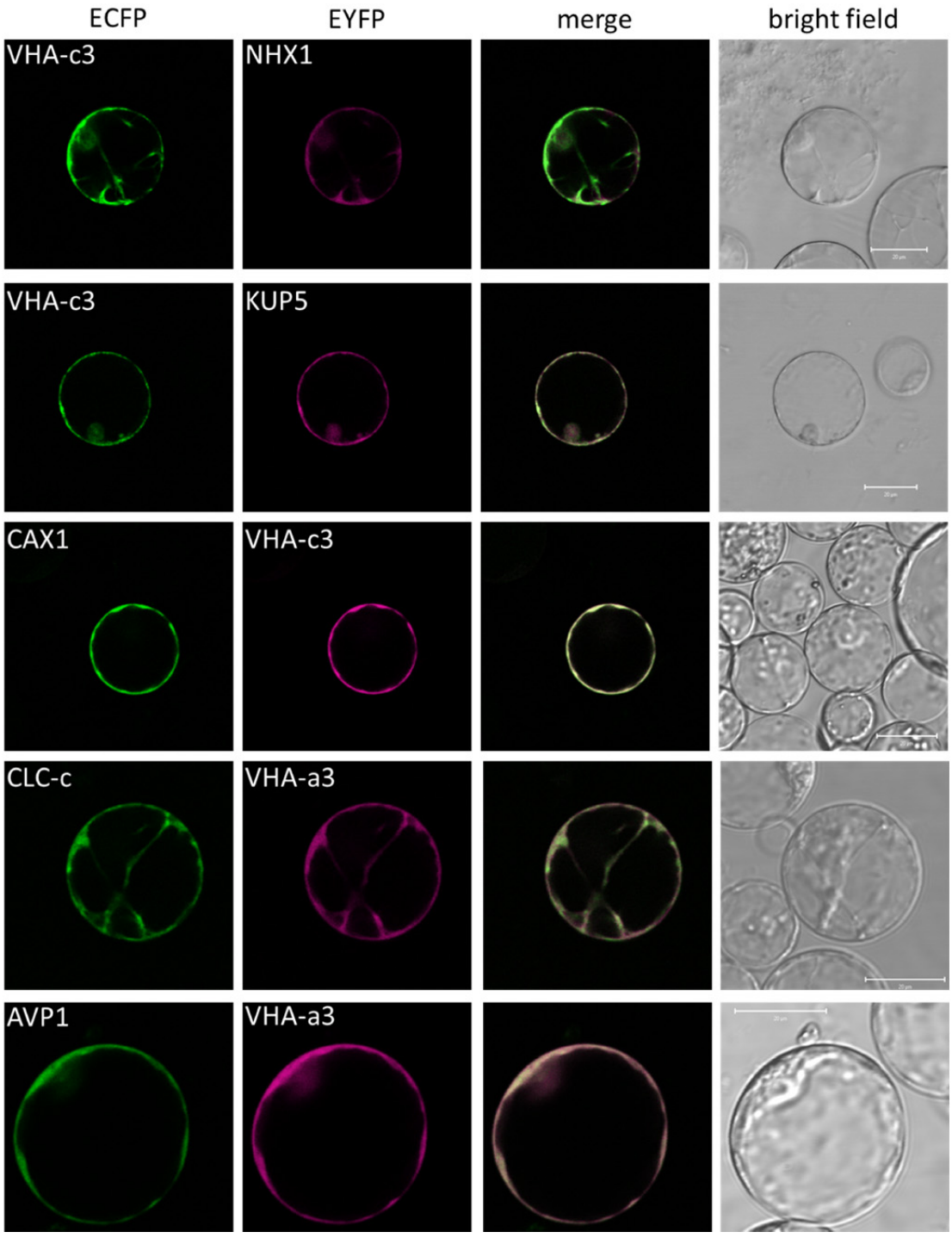

Figure 2. Co-localization of vacuolar transporters (NHX1, KUP5, CAX1, CLC-c, AVP1) and the membrane integral V-ATPase subunits VHA-c3/VHA-a3. All cells show the large central vacuole that occupies most of the cellular volume and results in the rim-like localization-pattern of the fluorescent proteins. ECFP-constructs are given in green, EYFP in magenta. Co-localized areas appear white in the merged image. Scale bar: 20 μm.

termini of VHA-a and VHA-c are exposed to the vacuolar lumen, VHA-c" and VHA-e do not reside at the tonoplast, and the role of VHA-d is still elusive, so that V_O-subunits did not qualify for mbSUS. Therefore, VHA-A and VHA-E1 were chosen as representatives of the hexameric head and the peripheral stalk, respectively. This approach was selected for the genes related to nitrate metabolism due to an undetectable expression of fluorescent protein-tagged nitrate reductase 2.

For mbSUS-analysis, the V-ATPase subunits VHA-A and VHA-E1 were fused to the N-terminal fragment of Ubiquitin (Nub), CLC-c and NR2 were fused to the C-terminal half of Ubiquitin (Cub). The yeast was selected for diploid cells carrying both Nub- and Cub-constructs. The selection relied on auxotrophy of the yeast strains. Finally, an x-gal assay of the yeast cells proved protein-protein interactions using the β–galactosidase as reporter gene. To this end, cells were lysed, the substrate X-gal was added and the turnover of X-gal by the β–galactosidase resulted in a blue staining. The assay revealed protein-protein interactions between VHA-E1/CLC-c and VHA-A/NR2, whereas it resulted in a lack of blue staining for VHA-A/CLC-c and VHA-E1/NR2 (Figure 3B).

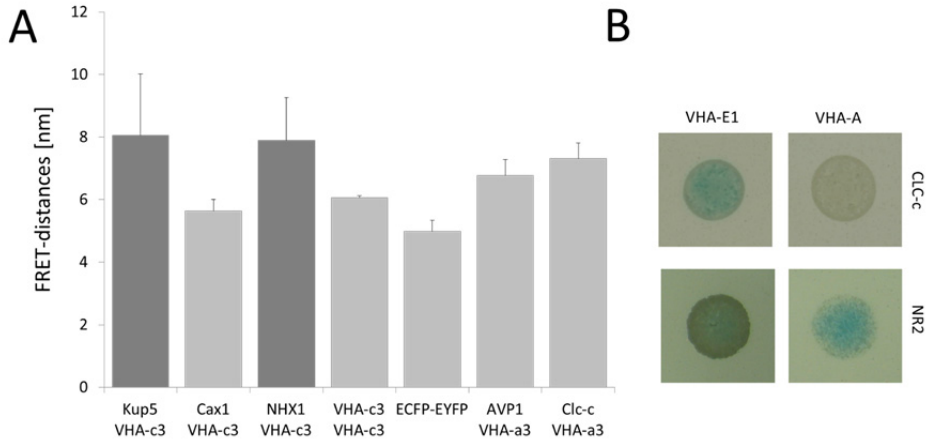

Figure 3. Protein-protein interactions between V-ATPase subunits and vacuolar transporters/nitrate reductase 2. A) FRET-derived distances of fluorescent proteins which were fused to proteins as indicated at the x-axis. Light grey columns show protein pairs with distances below 1.5-times R_0, dark grey columns those that exceeded 1.5-times R_0. The mean average ± standard deviation is given, n > 10. B) mbSUS X-gal assay. The interactions between NR2 and VHA-A, NR2 and VHA-E1, CLC-c and VHA-A and CLC and VHA-E1 were analyzed and a blue staining showed the turnover of X-gal by the reporter β–galactosidase. The expression level of the β–galactosidase depends on the strength of the analyzed protein-protein interaction. Representative images out of three independent experiments are shown for each combination.

3.3. Activity in insertion lines

The analysis of the insertion lines confirmed that the lines SALK_105121C (*nhx1*), SALK_120707C (*kup5*), SALK_115644C (*clc-c*), and SALK_106153C (*avp1*) were homozygous while the transgenic line SALK_021486C (*cax1*) was heterozygous. Unfortunately, the primer combination for genotyping the insertion line *clc-c* resulted in two products, but both PCR-products

obtained with the insertion line *clc-c* were distinct from the product obtained with the wildtype so that this transgenic line is homozygous. *avp*1 and *cax*1 showed a delayed germination in comparison to the wildtype Col-0: After 5 days 86.6% of the wildtype plants germinated, but only 76.1% of the *cax1*-line and 52.9% of the *avp1*-line germinated within five days. However, four weeks old plants of *nhx1*, *kup5*, *clc-c* and *avp1* did not show a significant difference to the wildtype, but the growth of *cax1*, though heterozygous, was significantly reduced (Figure 4). Next, the proton pumping activity was obtained by measuring the vacuolar pH in the plants. Vacuoles were loaded with 6-carboxyfluorescein, ratiometric images were taken with the two excitation wavelengths 458 nm and 488 nm using a confocal laser scanning microscope. The vacuolar pH was determined based on the obtained images. Significant effects of the t-DNA insertion were observed for *nhx1*, which showed an increase of pH by 1.38 units, and for *cax1*, which showed a decrease of vacuolar pH by 0.52 units (Figure 5). Since at least two proton pumps are active at the tonoplast, the V-ATPase activity was measured by the Bafilomycin-sensitive release of phosphate. The phosphate release was normalized to the protein content of the tonoplast samples. All three antiporter-lines showed a reduced V-ATPase activity, the symporter KUP*5* did not affect the activity and lack of the primary active proton pump AVP1 was compensated by an increase of V-ATPase activity (Figure 5).

3.4. Interplay of nitrate and V-ATPase activity

For simplicity, the heterotrophic Arabidopsis cell culture AT7 was applied to investigate the impact of nitrate on the vacuolar pH and the biomass yield. The strategy had been to analyze combinatory effects of nitrate as nitrogen source and inhibition of V-ATPase by bafilomycin to gain new insights into the interplay of nitrate assimilation and V-ATPase regulation. To this end increasing concentrations of either potassium nitrate as solely nitrogen source or bafilomycin as V-ATPase inhibitor were tested to identify concentrations that resulted in a minor but significant effect on biomass production. Such slight responses were seen for 60 mM potassium nitrate and 10 nM bafilomycin, respectively (table 3): five days after inoculation with 3 g of cell culture, the biomass was 12.3 ± 0.6 g for the control grown in MS-media, 10.2 ± 0.5 g for the supply of 60 mM KNO_3 and 11.1 ± 0.1 g for 10 nM bafilomycin. 40 mM KNO_3 resulted in an insignificant reduction of biomass (11.7 ± 0.3 g), 100 mM KNO_3 resulted in a strong reduction of biomass production (4.3 ± 0.1 g), 200 mM KNO_3 in cell death (1.8 ± 0.3 g). Addition of 5 nM bafilomycin gave 11.8 ± 0.5 g which was not significantly different from the control. Concentrations of 20 to 80 nM bafilomycin showed a significant reduction of biomass production to 8.5–3.4 g.

Next, the vacuolar pH was measured in response to these conditions as indicator of V-ATPase activity. The vacuolar pH was 6.73 ± 0.16 under control conditions (18.8 mM KNO_3 and 20.6 mM NH_4NO_3), 7.17 ± 0.17 in presence of 60 mM KNO_3 and 6.42 ± 0.03 with 10 nM bafilomycin. The response to 10 nM bafilomycin indicates rather a disturbance of pH-homeostasis than an inhibition of proton pumping at the tonoplast. The combination of 60 mM KNO_3 and 10 nM bafilomycin gave a vacuolar pH of 6.96 ± 0.21. To determine if this response to both 60 mM KNO_3 and 10 nM bafilomycin is an additive effect, the sum of the ΔpH-values of solely 60 mM KNO_3 and solely 10 nM bafilomycin was calculated in relation to the control and finally offset against the vacuolar pH at control conditions. This gave a vacuolar pH of 6.86 ± 0.2 what is close to the response obtained by

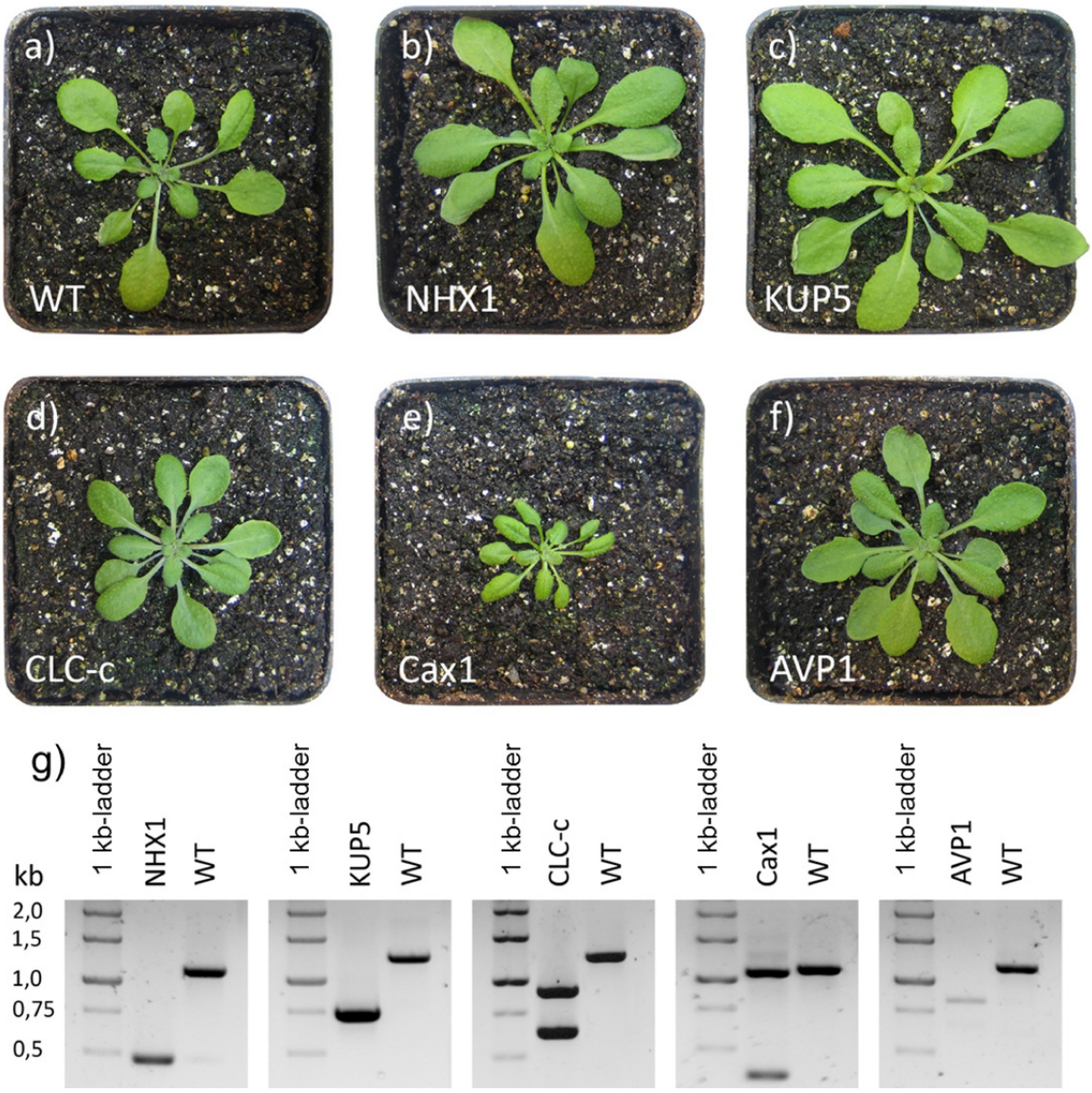

Figure 4. Phenotype of t-DNA insertion lines and wildtype Col-0 plants. Representative images are shown for the wildtype (a) and lines with insertions in the genes encoding for NHX1 (*nhx1*, b), KUP5 (*kup5*, c), CLC-c (*clc-c*, d), CAX1 (*cax1*, e) and AVP1 (*avp1*, f), respectively. More than 20 plants were analyzed and delayed growth was observed for *cax1*. Genomic DNA was isolated and the insertion was analyzed by PCR. To this end, three primers were applied: one binding to the insertion, two binding to the genomic sequences flanking the insertion. Wildtype samples resulted in a PCR-product of both flanking primers, samples from the insertion lines resulted in PCR-products of the primer binding to the insertion and one of the two flanking primers. *clc-c* showed two PCR-products which were both distinct in size from the wildtype PCR-product. It was concluded that one of the two PCR-products obtained with the *clc-c* was unspecific. Finally, genotyping revealed that all transgenic lines were homozygous except of *cax1* which was heterozygous (g). The heterozygous genotype of *cax1* was confirmed by sequencing of the PCR-products.

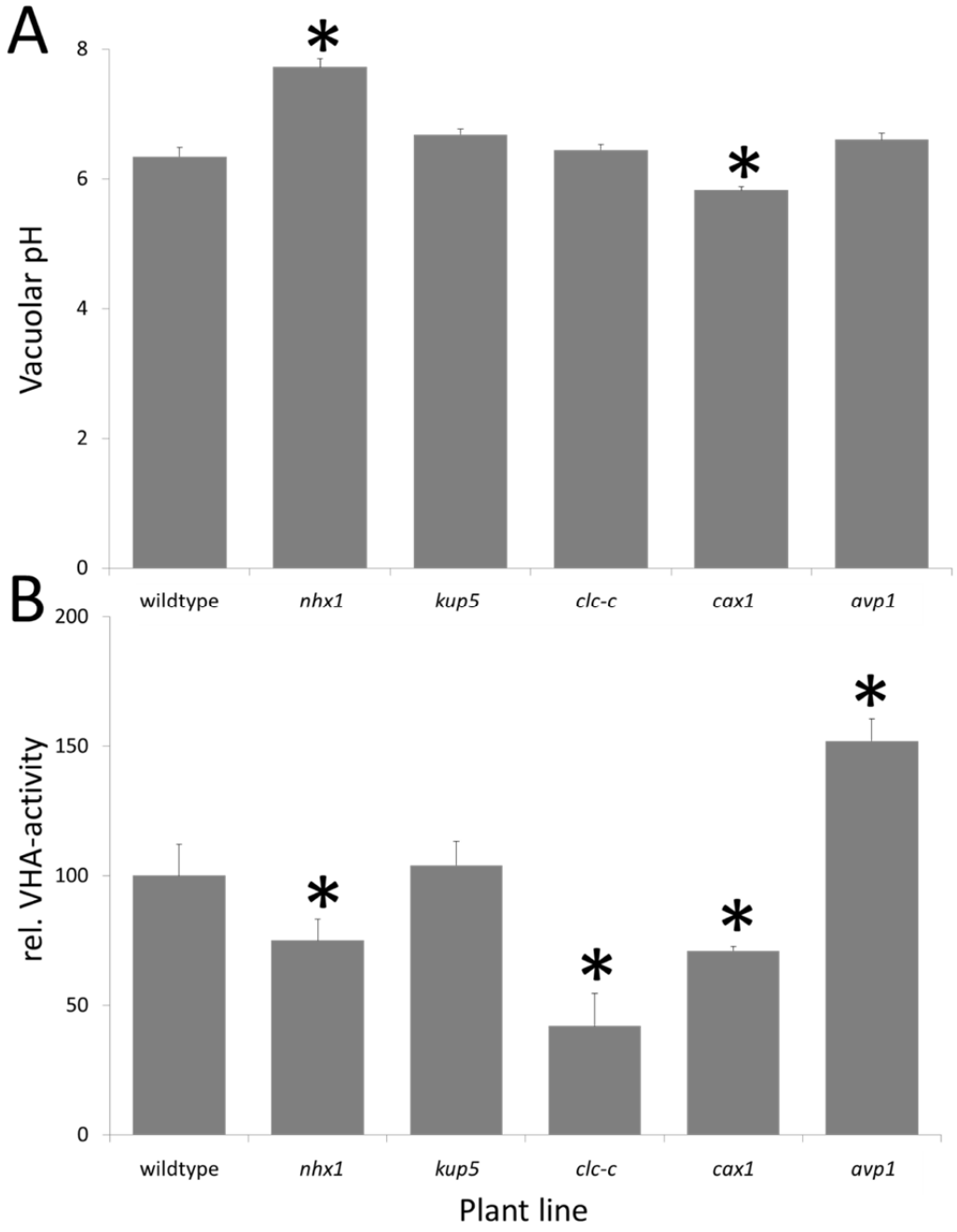

Figure 5. Vacuolar pH (A) and V-ATPase activity (B) in the transgenic lines and the wildtype Col-0. A) Vacuoles were loaded with the pH-responsive dye 6-carboxy fluorescein and pH was measured by imaging sequentially with the excitation wavelengths 458 nm and 488 nm using a confocal laser scanning microscope (mean ± SE is given, n = 30). B) V-ATPase activity was measured in leaf tonoplasts by bafilomycin-sensitive phosphate release. The data was normalized to the average activity of the wildtype plants (mean ± SE, n = 3). Asterisks mark significant differences between the transgenic lines and the wildtype ($p < 0.05$).

the experimental combination of 60 mM KNO_3 and 10 mM bafilomycin and indicates a simple additive effect of KNO_3 and bafilomycin. However, the data points to a slight overcompensation of the bafilomycin-induced V-ATPase inhibition, probably by the V-PPase, and an effective inhibition of vacuolar acidification by 60 mM nitrate, since the vacuolar pH is close to the cytosolic pH under these conditions. It should be noticed that in this cell type the pH-gradient between cytosol and vacuolar lumen was generally low.

Table 3. Impact of KNO_3 and bafilomycin on biomass production and vacuolar pH.

Effector	Biomass	Effector	vacuolar pH
MS-media	12.3 ± 0.6 g	MS-media	6,73 ± 0.16
40 mM KNO_3	11.7 ± 0.3 g	60 mM KNO_3	7.17 ± 0.17
60 mM KNO_3	10.2 ± 0.5 g	10 nM bafilomycin	6.42 ± 0.03
100 mM KNO_3	4.3 ± 0.1 g	60 mM KNO_3 & 10 nM bafilomycin	6.96 ± 0.21
200 mM KNO_3	1.8 ± 0.3 g	Σ 10 nM bafilomycin, 60 mM KNO_3	6.86 ± 0.2
5 nM bafilomycin	11.8 ± 0.5 g		
10 nM bafilomycin	11.1 ± 0.1 g		
20 nM bafilomycin	8.5 ± 0.7 g		
40 nM bafilomycin	5.6 ± 0.5 g		
80 nM bafilomycin	3.4 ± 0.4 g		

4. **Conclusion**

The secondary active transporters NHX1, KUP5, CLC-c and CAX1 and the proton pump AVP1 were tested for their interaction with the V-ATPase. The data demonstrated a physical interaction of CAX1, CLC-c and AVP1 with the V-ATPase, while proof of interaction failed for NHX1 and KUP5. The insertion line affecting AVP1 showed no effect on the vacuolar pH, but an increase of V-ATPase activity. It is concluded, that the V-ATPase compensates successfully for the lack of AVP1. While AVP1 is the dominant pump in younger cells and developing tissues, the V-ATPase is dominant in older tissues [8,10]. This distinct activity during plant development might explain that Li and coworkers (2005) [48] observed an increase of vacuolar pH in AVP1 knockout lines. The observed interaction of V-ATPase and AVP supports the idea of a functional interplay of V-ATPase and AVP1 that might be established at the stage of prevacuolar compartments [49] and which is mediated by a direct protein-protein interaction.

In general, NHX-activity reduces the vacuolar pH by exporting protons from the vacuole [50]. Interestingly, the knockout of NHX in yeast reduced the vacuolar pH, too [51], pointing to a more complex situation. Indeed, it has been reported before, that NHX1 is involved in the regulation of vacuolar pH and even a direct functional interaction of V-ATPase and NHX1 was described [52,53,54]. As FRET depends strongly on dipole-orientation of donor and acceptor, the low FRET-efficiencies measured here do not rule out a physical interaction between V-ATPase and NHX1. The same is valid for the vacuolar potassium ion/proton-symporter KUP5. However, an insertion in the gene encoding KUP5 had no effect on either the vacuolar pH or the V-ATPase activity, so that the coupling of primary and secondary active transport is evident for NHX1

but not for KUP5. It has to be considered that the tonoplast comprises a multitude of transport proteins, which modulate the membrane potential and pH-gradient, and thus, consume or contribute to the energy stored in the pmf. This complexity might have caused the apparent uncoupling of V-ATPase activity and vacuolar acidification in transgenic lines.

The interplay of V-ATPase and CAX1 has been intensively investigated since the nineties. The proton motif force generated by vacuolar proton pumps drives the calcium transport by CAX1 [55,56]. The relationship between both transporters appears mutual: While the calcium-transport depends on the pmf, the knockout of CAX1 resulted in reduced V-ATPase activity but increased AVP1-activity and overexpression of CAX1 led to a higher activity of the V-ATPase [57,58]. In *Catharanthus roseus*, the vacuolar pH was 5.6, if CAX-proteins were inactivated, and 6.2, if the transporters were active [59]. Based on this data a direct coupling of proton pumps and CAX1 was concluded but a physical interaction was not proven [60]. Due to the role of Ca^{2+} as important signaling molecule, the double-knockout of CAX1/CAX3 had an impact on plant growth, cell expansion, stomata opening and transpiration [45,61]. Within the present work, heterozygous lines showed a reduced V-ATPase activity and a reduced vacuolar pH, so that the reduced V-ATPase-activity does not simply result in an increase of AVP1-activity, it appears to be overcompensated by AVP1. The FRET-data indicates that the mode of bidirectional regulation is a physical interaction between the V_0-sector and CAX1. The FRET-efficiency, the strong impact of CAX1's knockdown on vacuolar acidification and the negligible degree of transcript correlation might further indicate that the interaction is not established during biosynthesis at the ER, at least not in a stable ratio or constitutive manner.

The connection between nitrate and V-ATPase appears contradictory: on the one hand, nitrate accumulation is a physiological consequence of higher nitrate levels [62]. On the other hand, nitrate is known to function as ATP-competitor and thus, inhibits V-ATPases [63] and the vacuolar nitrate accumulation by secondary active anion/proton exchangers depends on the activity of the V-ATPase. This contradiction of nitrate inhibition and required maintenance/stimulation of V-ATPase activity points to a nitrate concentration-dependent regulation of the V-ATPase, turning the V-ATPase on in response to a moderate increase of cellular nitrate concentration, while high nitrate concentrations inhibit the V-ATPase by blocking the ATP-binding sites. Nitrate and chloride are transported by members of the CLC-family, of which CLC-a, CLC-b and CLC-c are located at the tonoplast [6,64,65]. All three are known to function as antiporters [6,66]. The role of CLC-c is under discussion, initially identified as nitrate transporter, a more recent work stated that CLC-c functions as chloride transporter [6,67,68,69]. Within the present work, it could be shown that CLC-c interacts with the V-ATPase and an insertion within the gene encoding CLC-c resulted in a reduced V-ATPase activity, but only insignificantly increased vacuolar pH. This clearly demonstrates the tight relationship between both transporters, regardless of the substrate of CLC-c. The fact that endosomal V-ATPases co-localize with CLC-d [70] point to a general co-occurence of CLC-proteins and V-ATPases. The coupling of nitrate transport and V-ATPase becomes more evident by the observed interaction of V-ATPase and nitrate reductase 2. NR2 is the dominant nitrate reductase responsible for reduction of 90% of the cellular nitrate, only 10% is reduced by NR1 [71]. The activity of NR2 is highly induced and the vacuolar nitrate accumulation is reduced in leaves of the *vha2vha3*-mutant which lacks functional V-ATPases at the tonoplast and shows a vacuolar pH that is less acidic by only 0.5 units in root epidermal cells [10]. The higher cytosolic nitrate concentration is known to enhance NR-activity [72] and is related to the reduced vacuolar accumulation of nitrate. The data on

the vacuolar acidification differs from the data obtained here. The main difference between both data sets is the presence of an inhibited V-ATPase here and the lack of functional V-ATPases at the tonoplast in the previous work. One possible explanation is that compensation by the V-PPase requires the presence of the V-ATPase so that for instance the V-PPase can sense the activity state of the V-ATPase. On the other hand, high level of nitrate efficiently prevents vacuolar acidification without inducing any compensation, though nitrate is thought to interfere with ATP-binding and should not affect the V-PPase. Obviously, the coordination of vacuolar proton pumps is more complex and depends on multiple factors. Last but not least both V-ATPase and nitrate reductase are regulated in response to blue light via phosphorylation followed by binding of the regulatory 14-3-3 proteins [15,73]. This might contribute to the coordination of nitrate assimilation and nitrate transport, too.

Acknowledgement

This work was funded by the Deutsche Forschungsgemeinschaft (DFG), SFB613 TP A5, and Bielefeld University (Faculty of Biology). We are grateful to Karsten Niehaus and Thomas Patschkowski for helpful support in MALDI-MS.

Conflict of Interest

All authors declare no conflicts of interest in this paper.

References

1. Owens T, Poole RJ (1979) Regulation of cytoplasmic and vacuolar volumes by plant cells in suspension culture. *Plant Physiol* 64: 900–904.
2. Seidel T, Siek M, Marg B, et al. (2013) Energization of vacuolar transport in plant cells and its significance under stress. *Intern Rev Cell Mol Biol* 304: 57–131.
3. Tuteja N, Mahajan S (2007) Calcium signaling network in plants. *Plant Signal Behav* 2: 79–85.
4. Hirschi K (2001) Vacuolar H^+/Ca^{2+}-transport: who's directing the traffic? *Trends Plant Sci* 6: 100–104.
5. Miller AJ, Smith SJ (1992) The mechanism of nitrate transport across the tonoplast of barley root cells. *Planta* 187: 554–557.
6. Jossier M, Kroniewicz L, Dalmas F, et al. (2010) The Arabidopsis vacuolar anion transporter, AtCLCc, is involved in the regulation of stomatal movements and contributes to salt tolerance. *Plant J* 4: 563–576.
7. Fischer-Schliebs E, Mariaux JB, Lüttge U (1997) Stimulation of H^+transport activity of vacuolar H^+ATPase by activation of H^+PPase in *Kalanchoë blossfeldiana*. *Biologia Plantarum* 2: 169–177.
8. Taiz L (1992) The plant vacuole. *J Exp Biol* 172: 113–122.
9. Schnitzer D, Seidel T, Sander T, et al. (2011) The cellular energization state affects peripheral stalk stability of plant vacuolar H^+-ATPase and impairs vacuolar acidification. *Plant Cell Physiol* 52: 946–956.

10. Krebs M, Beyhl D, Gorlich E, et al. (2010) Arabidopsis V-ATPase activity at the tonoplast is required for efficient nutrient storage but not for sodium accumulation. *Proc Nat Acad Sci USA* 7: 3251–3256.
11. Smart LB, Vojdani F, Maeshima M, et al. (1998) Genes involved in osmoregulation during turgor-driven cell expansion of developing cotton fibers are differentially regulated. *Plant Physiol* 116: 1539–1549.
12. Grabe M, Wang H, Oster G (2000) The mechanochemistry of V-ATPase proton pumps. *Biophys J* 78: 2798–2813.
13. Konishi H, Yamane H., Maeshima M, et al. (2004) Characterization of fructose-bisphosphate aldolase regulated by gibberellin in roots of rice seedlings. *Plant Mol Biol* 56: 839–848.
14. Konishi H, Maeshima M, Komatsu S (2005) Characterization of vacuolar membrane proteins changed in rice root treated with gibberellin. *J Proteome Res* 4: 1775–1780.
15. Klychnikov OI, Li KW, Lill H, et al. (2007) The V-ATPase from etiolated barley (Hordeum vulgare L) shoots is activated by blue light and interacts with 14-3-3 proteins. *J Exp Bot* 58: 1013–1023.
16. Lu M, Ammar D, Ives H, et al. (2007) Physical interaction between aldolase and vacuolar H^+-ATPase is essential for the assembly and activity of the proton pump. *J Biol Chem* 282: 24495–24503.
17. McCubbin AG, Ritchie SM, Swanson SJ, et al. (2004) The calcium-dependent protein kinase HvCDPK1 mediates the gibberellic acid response of the barley aleurone through regulation of vacuolar function. *Plant J* 39: 206–218.
18. Hong-Hermesdorf A, Brüx A, Grüber A, et al. (2006) A WNK-kinase binds and phosphorylates V-ATP subunit C. *FEBS Lett* 580: 932–939.
19. Cohen A, Perzov N, Nelson, et al. (1999) A novel family of yeast chaperons involved in the distribution of V-ATPase and other membrane proteins. *J Biol Chem* 274: 26885–26893.
20. Holliday LS, Lu M, Lee BS, et al. (2000) The amino-terminal domain of the B subunit of vacuolar H^+-ATPase contains a filamentous actin binding site. *J Biol Chem* 275: 32331–32337.
21. Müller O, Neumann H, Bayer MJ, et al. (2003) Role of the Vtc proteins in V-ATPase stability and membrane trafficking. *J Cell Sci* 116: 1107–1115.
22. Bayer MJ, Reese C, Buhler S, et al. (2003) Vacuole membrane fusion: V_0 functions after trans-SNARE pairing and is coupled to the Ca^{2+}-releasing channel. *J Cell Biol* 162:211–222.
23. Vitavska O, Merzendorfer H, Wieczorek H (2005) The V-ATpase subunit C binds to polymeric F-actin as well as to monomeric G-actin and induces crosslinking of actin filaments. *J Biol Chem* 280: 1070–1076.
24. Cagnac O, Leterrier M, Yeager M, et al. (2007) Identification and characterization of Vxn1p, a novel type of vacuolar monovalent cation/H^+-antiporter of *Saccharomyces cerevisiae*. *J Biol Chem* 282: 24284–24293.
25. Smardon AM, Kane PM (2007) RAVE is essential for the efficient assembly of the C subunit with the vacuolar H(+)-ATPase. *J Biol Chem* 282:26185–26194.
26. Jones AM, Xuan Y, Xu M, et al. (2014) Border control- a membrane-linked interactome of Arabidopsis. *Science* 344: 711–716.
27. Arabidopsis Interactome Mapping Consortium (2011) Evidence for network evolution in an Arabidopsis interactome map. *Science* 333: 601–607.

28. Trezzini GF, Horrichs A, Somssich IE (1993). Isolation of putative defenserelated genes from *Arabidopsis thaliana* and expression in fungal elicitor-treated cells. *Plant Mol Biol* 21: 385–389
29. Alonso JM, Stepanova AN, Leisse TJ, et al. (2003) Genome-wide insertional mutagenesis of *Arabidopsis thaliana*. *Science* 301: 653–657.
30. Dietz KJ, Heber U, Mimura T (1998) Modulation of the vacuolar H+-ATPase by adenylates as basis for the transient CO2-dependent acidification of the leaf vacuole upon illumination. *Biochim biophys acta* 1373: 87–92.
31. Bencini DA, Shanley MS, Wild JR, et al. (1983) New assay for enzymatic phosphate release: application to aspartate transcarbamylase and other enzymes. *Anal Biochem* 132: 259–264.
32. Seidel T, Schnitzer D, Golldack D, et al. (2008) Organelle-specific isoenzymes of plant V-ATPae as revealed by in vivo-FRET analysis. *BMC Cell Biol* 9:928–928.
33. Seidel T, Golldack D, Dietz KJ (2005) Mapping of C-termini of V-ATPase subunits by in vivo-FRET measurements. *FEBS Lett* 579: 4374–4382.
34. Müller SM, Galliardt H, Schneider J, et al. (2013) Quantification of Förster resonance energy transfer by monitoring sensitized emission in living plant cells. *Front Plant Sci* 4:413.
35. Obrdlik P, El.Bakkoury M, Hamacher T, et al. (2004) K^+-channel interactions detected by a genetic system optimized for systematic studies of membrane protein interactions. *Proc Nat Acad Sci USA* 101: 12242–12247.
36. Gietz RD, Schiestl RH, Willems AR, et al. (1995) Studies on the transformation of intact yeast cells by the LiAc/SS-DNA/PEG procedure. *Yeast* 11: 355–360.
37. Ludewig U, Wilken S, Wu B et al. (2003) Homo- and hetero-oligomerization of ammonium transporter-1 NH4 uniporters. *J Biol Chem* 278: 45603–45610.
38. Seidel T, Kluge C, Hanitzsch M, et al. (2004) Co-localization and FRET-analysis of subunits c and a of the vacuolar H+-ATPase in living plant cells. *J Biotechnol* 112: 165–175.
39. Appelhagen I, Huep G, Lu, GH, et al. (2010) Weird fingers: functional analysis of WIP domain proteins. *FEBS Lett* 584: 3116–3122.
40. Schwacke R, Schneider A, Van Der Graaff E, et al. (2003) ARAMEMNON, a Novel Database for Arabidopsis Integral Membrane Proteins. *Plant Physiol* 131: 16–26.
41. Obayashi T, Nishida K, Kasahara K, et al. (2011) ATTED-II updates: condition-specific gene coexpression to extend coexpression analyses and applications to a broad range of flowering plants. *Plant Cell Physiol* 52: 213–219.
42. Joshi HJ, Hirsch-Hoffmann M, Baerenfaller K, et al. (2011) MASCP Gator: An aggregation portal for the visualization of Arabidopsis proteomics data. *Plant Physiol* 155: 259–270.
43. Winter D, Vinegar B, Ammar R, et al. (2007) An 'Electronic Fluorescent Pictograph' Browser for Exploring and Analyzing Large-Scale Biological Data Sets. *PLoS One* 2: e718.
44. Mäser P, Thomine S, Schroeder JI, et al. (2001) Phylogenetic relationships within cation transporter families of Arabidopsis. *Plant Physiol* 126: 1646–1667.
45. Cheng NH (2005). Functional Association of Arabidopsis CAX1 and CAX3 Is Required for Normal Growth and Ion Homeostasis. *Plant Physiol* 138: 2048–2060.
46. Silva P, Gerós H (2014) Regulation by salt of vacuolar H+ -ATPase and H+ -pyrophosphatase activities and Na+ /H+ exchange. *Plant Signal Behav* 4: 718–726.
47. Gadella T, Krogt G, Bisseling T (1999) GFP-based FRET microscopy in living plant cells. *Trends Plant Sci* 4: 287–291.

48. Li J, Yang H, Peer WA, et al. (2005) Arabidopsis H+-PPase AVP1 regulates auxin-mediated organ development. *Science* 310: 121–125.
49. Viotti C (2014) ER and vacuoles: never been closer. *Frontiers Plant Sci* 5:20.
50. Yoshida K, Miki N, Momonoi K, et al. (2009) Synchrony between flower opening and petal-color change from red to blue in morning glory, *Ipomoea tricolor cv.* Heavenly Blue. *Proc Japan Acad Series B, Physic biol sci* 85: 187–197.
51. Ali V, Shigeta Y, Tokumoto U, et al. (2004) An intestinalparasitic protist, *Entamoeba histolytica*, possesses a non-redundant nitrogen fixation-like system for iron-sulfur cluster assembly under anaerobic conditions. *J Biol Chem* 279: 16863–16874.
52. Gaxiola RA, Rao R, Sherman A, et al. (1999) The *Arabidopsis thaliana* proton transporters, AtNhx1 and Avp1, can function in cation detoxification in yeast. *Proc Nat Acad Sci USA* 96: 1480–1485.
53. Zhang Y, Wang L, Liu Y, et al. (2006. Nitric oxide enhances salt tolerance in maize seedlings through increasing activities of proton-pump and Na+/H+ antiport in the tonoplast. *Planta* 224: 545–555.
54. Bassil E, Tajima H, Liang YC, et al. (2011). The Arabidopsis Na+/H+antiporters NHX1 and NHX2 control vacuolar pH and K+ homeostasis to regulate growth, flower development, and reproduction. *Plant Cell* 23: 3482–3497.
55. Hirschi KD, Zhen RG, Cunningham KW, et al. (1996) CAX1, an H^+/Ca^{2+} antiporter from Arabidopsis. *Proc Nat Acad Sci USA* 16: 8782–8786.
56. Shigaki T, Pittman JK, Hirschi KD (2003) Manganese specificity determinants in the Arabidopsis metal/H+ antiporter CAX2. *J Biol Chem* 278: 6610–6617.
57. Cheng NH (2003) The Arabidopsis cax1 Mutant Exhibits Impaired Ion Homeostasis, Development, and Hormonal Responses and Reveals Interplay among Vacuolar Transporters. *Plant Cell* 15: 347–364.
58. Barkla BJ, Hirschi KD, Pittman JK (2014) Exchangers man the pumps. *Plant Signal Behav* 3: 354–356.
59. Guern J, Mathieu Y, Kurkdjian A, et al. (1989) Regulation of Vacuolar pH of Plant Cells II. A 31P NMR Study of the Modifications of Vacuolar pH in Isolated Vacuoles Induced by Proton Pumping and Cation/H+ Exchanges. *Plant Physiol* 89: 27–36.
60. Manohar M, Shigaki T, Hirschi KD (2011) Plant cation/H+ exchangers (CAXs): Biological functions and genetic manipulations. *Plant Biol* 13: 561–569.
61. Conn SJ, Gilliham M, Athman A, et al. (2011) Cell-specific vacuolar calcium storage mediated by CAX1 regulates apoplastic calcium concentration, gas exchange, and plant productivity in Arabidopsis. *Plant Cell* 23: 240–257.
62. McIntyre GI (1997) The role of nitrate in the osmotic and nutritional control of plant development. *Austral J Plant Physiol* 24: 103–118.
63. Randall SK, Sze H (1986) Properties of the partially purified tonoplast H+-pumping ATPase from oat roots. *J Biol Chem* 261: 1364–1371.
64. De Angeli A, Monachello D, Ephritikhine G, et al. (2006) The nitrate/proton antiporter AtCLCa mediates nitrate accumulation in plant vacuoles. *Nature* 442: 939–942.
65. Fecht-Bartenbach J, Bogner M, Dynowski M, et al. (2010) CLCb-mediated NO-3/H+ exchange across the tonoplast of Arabidopsis vacuoles. *Plant Cell Physiol* 51: 960–968.

66. Wudick MM, Luu DT, Maurel C (2009) A look inside: localization patterns and functions of intracellular plant aquaporins. *New phytol* 184: 289–302.
67. Geelen D, Lurin C, Bouchez D, et al. (2000). Disruption of putative anion channel gene AtCLC-a in Arabidopsis suggests a role in the regulation of nitrate content. *Plant J Cell Mol Biol* 21: 259–267.
68. Harada H, Kuromori T, Hirayama T, et al. (2004) Quantitative trait loci analysis of nitrate storage in Arabidopsis leading to an investigation of the contribution of the anion channel gene, AtCLC-c, to variation in nitrate levels. *J Exp Bot* 55: 2005–2014.
69. Miller AJ, Fan X, Orsel M, et al. (2007) Nitrate transport and signalling. *J Exp Bot* 58: 2297–2306.
70. Fecht-Bartenbach J, Bogner M, Krebs M, et al. (2007) Function of the anion transporter AtCLC-d in the trans-Golgi network. *Plant J* 50: 466–474.
71. Wilkinson JQ, Crawford NM (1991) Identification of the Arabidopsis CHL3 gene as the nitrate reductase structural gene NIA2. *Plant Cell* 3: 461–471.
72. Trewava A (1983) Plant growth substances—Metabolic flywheels for plant development. *Cell Biol Intern Rep* 7: 569–575.
73. Kaiser WM, Weiner H, Huber SC (1999) Nitrate reductase in higher plants: A case study for transduction of environmental stimuli into control of catalytic activity. *Physiologia plantarum* 105: 384–389.

AIMS Press